Energy profiling and planning and multi-objective optimization algorithms comparison performance

D Mitropoulou, MSc[a*], D *Dembinskas, MSc[a] ,Dr T. Miao, PhD[a]*
[a]RH Marine Netherlands BV, The Netherlands;
*Corresponding author. Email: <u>despoina.mitropoulou@rhmarine.com</u>

Synopsis

The modernization of naval ships requires continuous advancements in technology to ensure adaptability, sustainability, extended range, and reliability. In response to these challenges, the naval shipbuilding sector has adopted key technology trends, particularly in the fields of automation and the design of integrated, smart cyber-physical systems. As part of this development a research in the performance evaluation of a previously developed novel Energy Management and Control System (EMS) is performed, to ensure the smooth operational capabilities of naval vessels, addressing the necessity of designing high-performance ships for all operating conditions.

This paper aims to build upon the developments by exploring the potential benefits of integrating different multi-objective optimization algorithms into the EMS of naval ships. The traditional focus on fuel cost savings in current energy management systems may not fully handle the versatility of naval vessels, as each mission entails distinct operational requirements. The ability to adapt to a wide variety of missions in a continuous changing world underscores the importance of developing more sophisticated integrated control algorithms with multiple optimization goals. Yet, complexity can have an impact in terms of performance, and simplicity can be of great importance when choosing the most optimal optimization algorithm.

The proposed review is focusing on the performance comparison between four optimization algorithms: Lagrange-multiplier, Nelder Mead, interior point and active set and analyses the performance in terms of cost and computing time when optimizing shipboard energy production in a hybrid propulsion plant with a hybrid power supply. It considers the trade-off between multiple and conflicting operating goals, including fuel savings, maintenance costs, noise, and IR of on-board assets. To ensure equitable comparisons, a previously developed model of an Offshore Patrol Vessel, as published in INEC 2020 with title "Multi-objective optimization and Energy Management: adapt your ship to every mission" has been employed for testing and benchmarking purposes. Simulation results under varying operational profiles highlight the applicability, validity, and advantages of different EMS algorithms compared to conventional rule-based strategies currently in use.

Keywords: Energy Management; Hybrid propulsion; Multi-objective optimization; Algorithms performance

1.   Introduction

The introduction of increasingly smart automation systems and advanced user interfaces has facilitated more precise operational information onboard, enabling integrated system configuration management advice. Using data from interconnected management systems such as the Integrated Mission Management System (IMMS), Signature Management System, and Integrated Platform Management System (IPMS), ships can achieve optimized behaviour and performance tailored to their holistic operational demands.

For instance, selecting the optimal propulsion plant configuration across various operational conditions can lead to reductions in signatures (including noise and Infra-Red (IR)), Life Cycle Costs (LCC) (including maintenance and fuel consumption), and exhaust emissions. Additionally, new objectives with respect to the ship's operational mode, like optimized route planning or just-in-time arrival can be implemented, considering the most efficient route.

Optimization is particularly applicable to systems where operational choices exist regarding power generation, distribution, and/or consumption with more than one type of source like combination of a diesel generator with a battery device, e.g. hybrid power generation and propulsion plants. In such systems, power can be generated from different sources/storage devices and can be used to propel the vessel through various means, allowing for flexibility in energy generation, distribution, and consumption. Each mission's specific optimization goals and priorities and load profile influence these choices, determining the vessel's optimal operating point.

Authors' Biographies
D. Mitropoulou obtained a master's degree in electrical engineering at the National Technical University of Athens and a master degree in Sustainable Energy Technology from Delft University of Technology. She is the manager of Power Systems department at RH Marine.
D. Dembinskas obtained a bachelor's degree in electrical and Electronics engineering at the Siauliai University of Lithuania, a master degree in Electrical engineering at Delft University of Technology and a master degree in Wind energy at Norwegian University of Science and Technology. He is a Consultant of Power Systems department at RH Marine.
T. Miao obtained his PhD in Engineering Technology from the KU Leuven, with the topic of autonomous sailing, a master degree in Maritime Engineering from the Norwegian University of Science and a master degree in Maritime Engineering from the Royal Institute of Technology. He is a consultant at RH Marine.

As previously mentioned (Mitropoulou, et al., 2020) , current technology enables momentary automated optimization of electric power generation, primarily focused on fuel savings (Breijs & Amam, 2016) (Geertsma, Negenborn, Visser, & Hopman, 2017) (Kalikatzarakis, Geertsma, Boonen, Visser, & Negenborn, 2018). The significant value of such optimization algorithms has been demonstrated through various project results, indicating the potential for further gains by incorporating multiple optimization goals. Building upon this, efforts have been made to optimize ship operation towards minimal total cost of ownership (TCO) by accounting for battery lifetime in the control system (Mitropoulou & Elling, 2018).

For this paper in order to conduct the performance comparison between the four different optimization algorithms: Lagrange-multiplier, Nelder Mead, interior point (Lagrange-based), and active set (Lagrange-based), and analyse the performance in terms of cost and computing time, tests were conducted on all four aforementioned algorithms. These tests were applied across three sailing scenarios, entailing differing power demands and limitations, as well as diverse weight factor configurations. Notably, the Lagrange multiplier algorithm is currently employed in our existing Rhodium Energy Management System (EMS). Our objective is to distinguish and analyse the differences between the Lagrange method and the newly tested approaches, thereby informing and directing our future research and development efforts. It is important to acknowledge a minor deviation in this analysis: we incorporated nonlinear models in the constraints (specifically pertaining to the battery and electrical motor). Consequently, we employed numerical implementation to approximate the optimal solution point, as opposed to traditional analytical resolution techniques involving matrix calculations.

Section 2 provides a description of the studied system, focusing on a single system to illustrate the proposed EMS and demonstrate its feasibility.

Section 3 outlines the optimization objectives and constraints considered.

Section 4 discusses how to integrate multiple conflicting objectives into a single optimization goal, with different solution methods described.

Section 5 presents case studies comparing the proposed solution method to a baseline, demonstrating its validity.

Finally, conclusions, discussions, and results on dynamic profiles are provided in subsequent sections.

2. Description of the system

The research work puts emphasis on several optimisation strategies for the Energy Management System. The optimisation strategies are selected in the way that they can be adapted to every configuration of the power plant and propulsion plant. This research case focuses on previously adapted single line model (Mitropoulou, et al., 2020) which is presented in Figure 1.

The single line consists of the following objects:

- Main engines (ME) 2x each 9.1 MW nominal power and connected to its own shaft and propeller
- Diesel generators (DG) 4x each have rated power of 2.45 MW
- Battery banks (BB) 2x each with a capacity of 1 MWh with a maximum discharge/charge rate of 5C, resulting in 5 MW.
- Electric motors (EM) 2x each with a rated power of 3 MW with power take in (PTI) and power take off (PTO) capability.

Figure 1 represents the single line divided into three segments: propulsion, DC distribution and AC distribution. Going from the top of the diagram, which is the propulsion section consists of the main engines, gearboxes with the clutches, electric motors, with a capability of the power take in and power take out, and controllable pitch propellers. The middle position of the single line consists of the DC distribution network, which includes diesel generators connected to rectifiers and then to the DC switchboards. These switchboards supply power to several rectified auxiliary loads. The efficiency of all converters are taken into account including a factor of the power flow direction, which means that power is delivered or absorbed. The bottom section illustrates the low-voltage AC distribution and corresponding AC auxiliary loads.

For the fare comparison and following aforementioned developments the control diagram is kept as well the same aboard the vessel, which is depicted in Figure 2. This study centers on the energy management system (EMS), represented as the tertiary control loop. Information is transmitted from the EMS to both the primary control layers, namely the converters, governors, and active voltage regulators (AVRs), and the secondary control layers, including the power management system (PMS), propulsion control system (PCS), and battery management system (BMS). The PCS provides inputs to the main propulsion system, such as power and speed set points for the ME and PTI, as well as pitch control for the propeller. In instances where the motor operates as a shaft generator (i.e., PTO), it receives its power and speed set points from the PMS. Inputs for the PCS are derived from lever position, autopilot data, and dynamic position (DP) information, culminating in a virtual shaft speed set point. This set point, along with actual shaft power feedback from the PCS, is provided to the EMS.

The EMS provides power setpoints to the batteries and PTOs, diesel generators receive power and speed setpoints. Positioned one control level below the EMS, the PMS is tasked with distributing power setpoints based on load demand. In its turn, the PMS provides the auxiliary power feedback to the EMS. One level above the EMS, the integrated mission management system (IMMS), which consist of the mission planning and signature management systems. These systems translate operational modes into weight factors, as well as constraints and provides them to the EMS. In addition, supplementary information, including load prediction profiles, is supplied by various third-party applications through a high-level control system like integrated platform management system (IPMS) to the EMS.
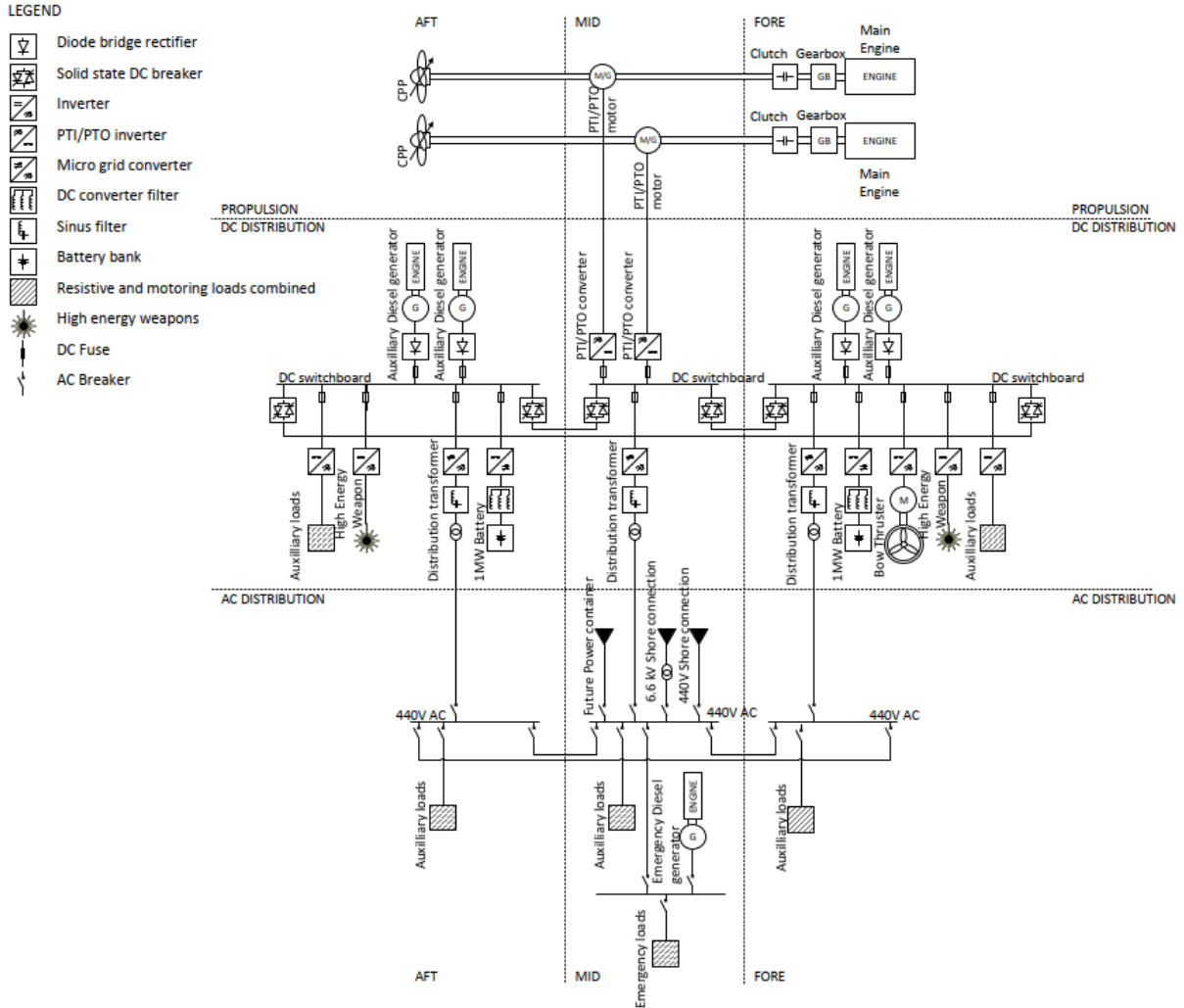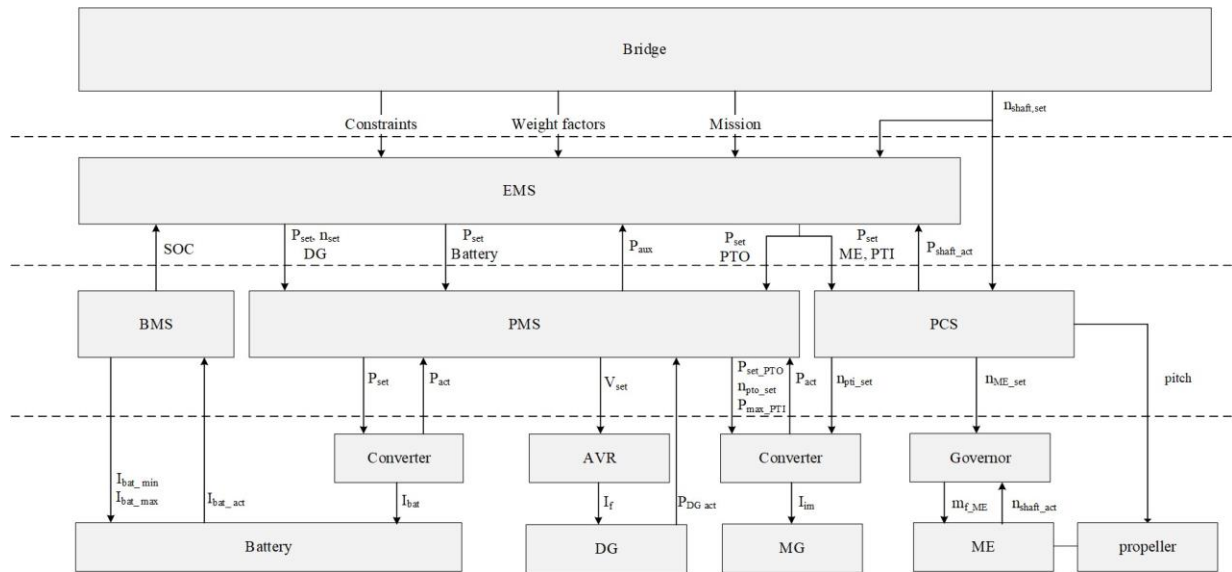

Figure 1: Single line diagram

Figure 2: Control diagram

## 3. Definition of the optimization problem

This section describes the optimisation goals that are implemented in the different algorithms. As mentioned in the research (Mitropoulou, et al., 2020), this continuation of the previous work utilises the same operational constrains, goals for the optimisation and total objective function. In the further subsections, the operational constrains, the goals for the optimisation and the objective function will be briefly explained.

One thing must be kept in mind, sometimes different or even conflicting goals are defined. They consist of the following: Fuel consumption, life cycle cost (LCC), Noise and Infra-red signature (IR). The importance of the goals is defined by the weight factors. These weight factors are an input to the system from the user or the IMMS system and closely depend on the mission and operational requirements.

3.1. Model set-up and constraints

3.1.1. Fuel Consumption

In order to optimize the system with respect to fuel consumption, we consider the fuel consumed by the main engines (MEs) and diesel generators (DGs). Additionally, we represent the batteries with a virtual fuel consumption. This approach is focusing on optimizing the equipment's set points for the current moment, without considering past or future states. Batteries, however, inherently manage energy storage over time, meaning the energy they store must have required fuel used for charging in the past. Moreover, charging the battery now incurs a fuel cost, but it can save fuel in the future by discharging instead of using the DGs or MEs for power generation. Therefore, we account for a virtual fuel cost when using the batteries.
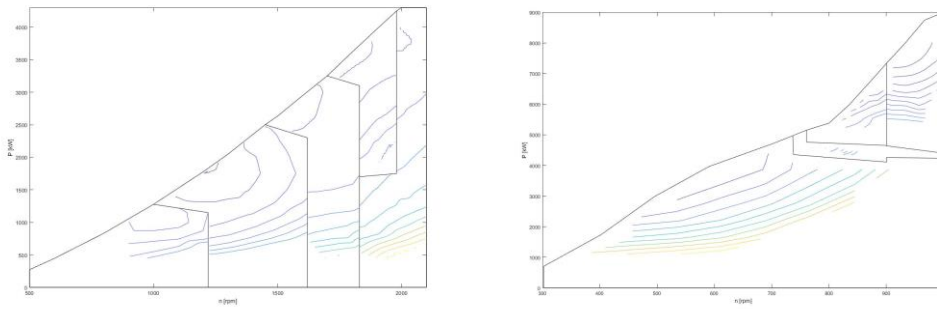
a. Auxiliary DG   b. ME

Figure 3: Auxiliary DG (left) and Main engine (right) fuel maps (in g/s)

Fuel consumption for the DGs and MEs is determined by using fuel maps, illustrated in Figures 3(a) and 3(b), respectively. The DG fuel map is divided into five regions, and the ME map into four, each delineated by black bounding boxes. These maps feature isolines representing fuel consumption rates (in grams per second). To estimate consumption from these maps, we fitted polynomial functions to each region. This process yielded a function,

$$f_{fuel,com,reg} = \sum_{j=0}^{J} \sum_{k=0}^{K} a_{,com,reg,j,k} n^j P^k, \tag{1}$$

where $a_{,com,reg,j,k}$ are the coefficients for the polynomial for component com operating in region reg. Furthermore n is the speed of the component and P its power output. Also, J and K are the degrees of the polynomial in the speed and power respectively. To integrate the battery's fuel cost, we use two equivalence factors, Eq_{char} and , Eq_{disc} which represent the expected future fuel savings per unit of energy charged into the battery now, while estimates the fuel previously consumed to charge each unit of energy. Different use cases were simulated with different equivalent factors and from these cases the better battery utilization was at lower Eq factors.
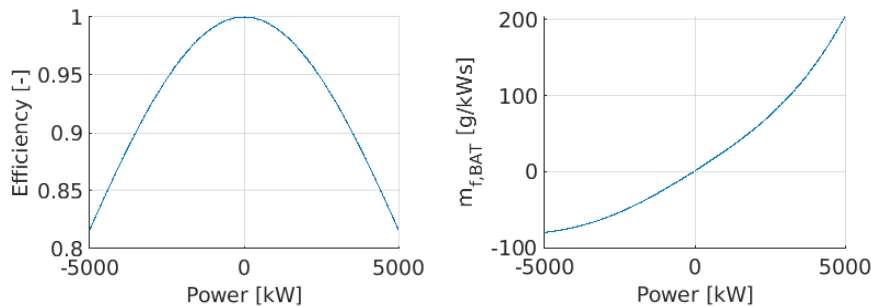
a) Efficiency   b) Equivalent fuel consumption

Figure 4: Battery efficiency and equivalent fuel consumption.

The battery's fuel cost is determined by multiplying the energy charged or discharged by the respective equivalence factor, depending on whether the battery is charging or discharging. Figures 4(a) and 4(b) show the battery efficiency and the resulting equivalent fuel consumption using $Eq_{char} = Eq_{disc} = 0.025$, which because of simulations proved to be optimal value for the best battery utilisation.
To determine the total fuel consumption of the system, we sum the fuel consumption of each individual component.

3.1.2. LCC

Regarding the LCC goal of the optimization, the focus was primarily on the main engines (MEs), diesel generators (DGs), and batteries, as these components were identified as the most critical contributors to the overall cost. The LCC for the MEs and DGs was modelled by incorporating a fixed operational cost, along with a cost

component that varies linearly with the speed of the respective ME or DG. This relationship can be expressed as follows for any given ME or DG.

$$f_{LCC,i} = a_{fixed} + a_{speed}n \; if \; P > 0, \tag{2}$$

where the coefficients are given by a_{fixed} and a_{speed} .

The Life Cycle Cost (LCC) of the battery was modelled with higher complexity due to the several factors that affect its lifetime. Battery degradation is influenced by the amount of power drawn from it and its current State of Charge (SoC). Additionally, discharging the battery when its SoC is low leads to greater damage. This relationship is depicted in Figure 5, which illustrates the LCC model for the battery. It is important to highlight that, for the purposes of this model, we assumed that charging does not significantly contribute to battery damage. The LCC of battery i were modelled using:

$$f_{LCC,i} = \frac{\Delta Damage_i a_{rpl} 3600}{\Delta t} + a_{fixed} \; if \; P_i \neq 0, \tag{3}$$

here $\Delta Damage_i$ is the damage incurred by the discharging of the battery, a_{rpl} is a coefficient representing the replacement costs of the battery and a_{fixed} is a fixed cost for operating the battery. Furthermore, Δt is the aforementioned time at which the system is expected to operate with the given operational values. To calculate the damage incurred by discharging the battery at certain SoC levels, the following model is used.

$$CTF(DoD) = \sum_{i=0}^{4} a_i DoD^{-i}, \tag{4}$$

Figure 5: Battery lifecycle cost

where $CTF(DoD))$ are the current number of cycles to failure depending on the depth of discharge DoD and a_i are model coefficients. The EMS keeps track of the current DoD and calculates the new expected DoD using the currently calculated settings. The damage to the battery, is calculated using:

$$Damage = \frac{1}{CTF(DoD)\varepsilon}, \tag{5}$$

where ε is a factor based on the current charge rate or current discharge rate of the battery (Li, et al., 2017) . The previous level of degradation of the battery is continuously monitored, and the expected new degradation is calculated based on the current operating conditions of the battery. The degradation difference ($\Delta Damage$) is then determined by subtracting the old degradation value from the new degradation estimate.

3.1.3. Noise

The noise optimisation goal was modelled for both the main engines and the diesel generators. Due to the lack of availability of maps on the engine noise relative to speed and power, an assumption of the maps was generated, and they were based on expert inputs as shown in Figure 6(a) and Figure 6(b) for the ME and DG noise, respectively. The main assumption is that the MEs contain resonance frequencies and thus produce the highest noise levels at 500 and 900 rpm at 95 dB. The noise generation at the lowest and highest speed (400 and 1000 rpm) are the lowest, which is about 20 dB lower. Furthermore, there is another dip in noise output at 750 rpm, with a reduction of about 10 dB compared to the peak value. These values are then further scaled based on power output, which means more power relates to higher noise output. The same assumptions were made for the diesel generators, where the values were scaled for the different speed envelopes of the DGs.
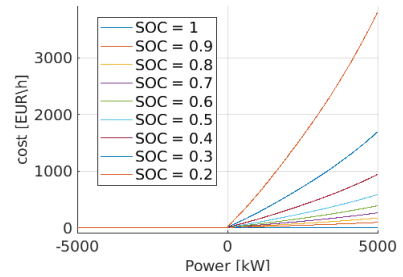
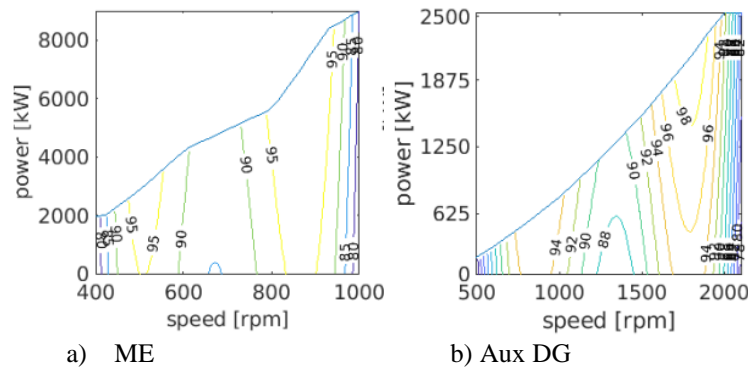a) ME   b) Aux DG

Figure 6: Noise maps

As with the fuel consumption, the produced noise was approximated by component *com* using a polynomial as presented:

$$f_{noise,com} = \sum_{j=0}^{J} \sum_{k=0}^{K} a_{com,j,k} \, n^j P^k, \tag{6}$$

here n and P are the speed and power of the component and $a_{com,j,k}$ are the coefficients for the polynomial utilised to model the component's noise. These results were obtained with approximations similarly as for the fuel maps.

The overall system noise was obtained by taking the maximum of the modelled noise output on all main engines and diesel generators in this system. So that, the resulting noise of the system is the noise output of the loudest component.

3.1.4. IR

As previously mentioned in the previous paper (Mitropoulou, et al., 2020) the infrared goal is considered being produced by the main engines only. The model map of the IR output for a ME is based on speed and power and was generated using a high fidelity model (Kalikatzarakis, Geertsma, Boonen, Visser, & Negenborn, 2018). The resulting model map was approximated using a polynomial function and was separated into two regions, which is given in Figure 7. This resulted in a modelled IR output of ME i operating in region reg given by function:

$$f_{IR,i,reg} = \sum_{j=0}^{J} \sum_{k=0}^{K} a_{j,k,reg} \, n^j P^k, \tag{7}$$

here n and P are the speed and power output of the main engine, respectively. Furthermore, $a_{j,k,reg}$ are the coefficients of the polynomial in region reg.
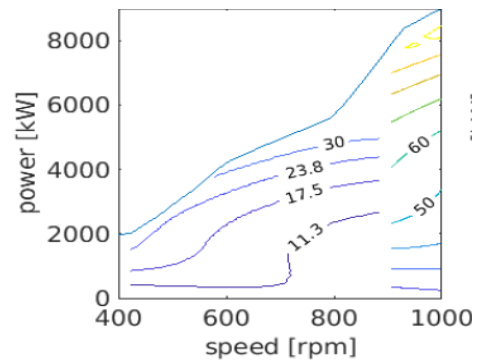

Figure 7: Main engine IR map

3.1.5. Total objective function

To incorporate these goals of fuel, LCC, noise and IR together the following approach is utilised. This is because calculated goals output values in different domains. As an example, fuel consumption is calculated in grams per second, where noise levels are outputted in decibels. Therefore, for the better comparison of the different objectives, these are normalised. The normalisation is followed by multiplication of each objective by a weight factor. The weight factors can take a value within [0-1] and sum up to 1. Resulting in a total objective function which is obtained by summing each normalised and weighted goal. As it can be observed below, the total objective function is given by:

$$f_{obj}(x) = w_{fuel} \frac{f_{fuel}}{f_{fuel}^{norm}} + w_{LCC} \frac{f_{LCC}}{f_{LCC}^{norm}} + w_{noise} \frac{f_{noise}}{f_{noise}^{norm}} + w_{IR} \frac{f_{IR}}{f_{IR}^{norm}}, \tag{8}$$

here, $f_{fuel}, f_{LCC}, f_{noise}$ and f_{IR} are calculated as described above and depend on the decided control values P_{ME}, P_{DG}, n_{DG}, P_{EM}, and P_{bat}). The normalization factors $f_{fuel}^{norm}, f_{LCC}^{norm}, f_{noise}^{norm}$ and f_{IR}^{norm} are computed as follows. A baseline is calculated for a given set of inputs. This set is the control inputs, when the battery is not used, and the propulsive power is generated as much as it can be possible by the MEs. The DGs generate power to support the electric loads and a minimum number of DGs is utilised. The electric motors are used in motoring mode when the main engine, which shares a shaft with the electric motor, is unable to provide sufficient propulsive load on its own. In situations where any of the electric motors demand additional power, the diesel generators would increase their output to supply the load. This baseline configuration establishes the initial values for various optimization goals. These baseline values are then used as normalization factors, allowing each objective to be measured as a relative increase or decrease from the baseline. This normalization ensures that different objectives are comparable on a common scale.

4. Optimisation algorithms

Four algorithms were investigated in this paper. The main purpose of the investigation was performance and total cost. The optimisation algorithms are listed below with a brief introduction.

4.1. Lagrange multiplier

The Lagrange multiplier algorithm is a method used for solving constrained optimization problems. It works by creating a Lagrangian function, which combines the original objective function with the constraints, each multiplied by a Lagrange multiplier. This function is then analyzed by taking its derivatives and setting them to zero to find critical points. Solving these resulting equations provides values that meet both the gradient of the original function and the constraints simultaneously. By evaluating the original objective function at these critical points, one can determine the maximum or minimum values within the given constraints. This algorithm is extensively used across various scientific fields due to its efficiency in addressing optimization problems that involve constraints.

4.2. Interior-Point Algorithm

Interior-point algorithms are advanced optimization techniques grounded in principles of convex optimization and numerical analysis. These methods solve constrained optimization problems by iteratively refining solutions within the feasible region's interior. They use barrier functions to ensure constraints are fulfilled throughout the process. Using sophisticated numerical methods and linear algebra, interior-point algorithms navigate complex, high-dimensional solution spaces. Their robustness and efficiency make them invaluable for optimizing complex systems under constraints, applicable in several fields such as engineering, economics, and finance.

4.3. Active-Set Algorithm

The active-set algorithm is a specialized numerical optimization method designed for solving nonlinear constrained problems, particularly those with a few active constraints compared to the total set. It iteratively converges on solutions by concentrating computational resources on the active constraints that are binding or nearly binding. This approach aims to minimize a quadratic approximation of the objective function. During the process, the algorithm updates the active set based on any newly identified constraints that are violated. Convergence is achieved when criteria like optimal conditions or specific tolerances are met. The strength of this algorithm lies in its ability to exploit the sparsity of active constraints, making it well-suited for problems with a limited number of such constraints. However, it may struggle with large-scale problems or dynamically changing constraint sets, often necessitating the use of alternative methods like interior-point algorithms or sequential quadratic programming.

4.4. Nelder-Mead Algorithm

The Nelder-Mead algorithm, also known as the simplex or downhill simplex method, is a technique for nonlinear optimization, particularly effective for smooth but potentially non-convex objective functions. It starts by forming a simplex in the parameter space, typically centered around an initial guess of the optimal solution. The algorithm iteratively evaluates the objective function at each vertex of the simplex and adjusts the simplex through operations like reflection, expansion, contraction, or shrinkage to explore the parameter space and improve the solution. Convergence is achieved when the objective function meets a predefined tolerance level or when the simplex's size sufficiently decreases. While the Nelder-Mead algorithm is appreciated for its simplicity and independence from gradient information, it can converge slowly, especially in high-dimensional or poorly conditioned scenarios, and it does not guarantee finding a global optimum. Despite these limitations, its flexibility and effectiveness across a wide range of optimization problems have led to its widespread use.

5. Simulation & Evaluation

5.1. Simulation

Simulations were conducted in Matlab to compare the energy-saving performance and computing time of the aforementioned four algorithms. All simulations were performed on a Windows 10 system running on a laptop equipped with an Intel i9 processor. The ship model used in the simulation is based on a previously developed model of an Offshore Patrol Vessel. We defined three scenarios, representing different missions from low to high energy requirements in order to test the algorithms. These settings are derived from previous work and correspond with those presented in the paper published by RH Marine, Damen, and TNO (Mitropoulou, et al., 2020). The normalization factors of the cost function are used to obtain the equivalent cost for different aspects and remain consistent across all scenarios and have been defined based on the parameters provided in the table.

The specifications of each scenario are listed in Table 1, including the ship's current state (initial state for optimization, such as ship speed, shaft speed, and State of Charge (SoC) of the battery bank), power demands and certain properties (e.g., the battery's equivalent charge and discharge factors).

Table 1: Current ship states and demands for three scenarios

Parameters	unit	Scenario		
		1	2	3
Ship speed	knot	20	20	20
Shaft speed - portside	rpm	75	97	129
Shaft speed - starboard	rpm	75	97	129
Shaft power demand - ps	kW	1710	3650	8640
Shaft power demand - stb	kW	1710	3650	8640
Auxiliary loads	kW	1650	1650	1650
State of charge of battery 1	-	0.7	0.7	0.7
State of charge of battery 2	-	0.7	0.7	0.7
Equivalent charge factor	-	0.035	0.035	0.035
Equivalent discharge factor	-	0.035	0.035	0.035
Safety margin	-	0.99	0.99	0.99
Normalization factor - fuel	-	293.8110		
Normalization factor - LCC	-	146.3675		
Normalization factor - noise	-	94.4147		
Normalization factor - IR	-	44.3437		

A notable feature of our testing methodology is that the on/off statuses of the main engines (MEs) and diesel generators (DGs) are not directly modified within the algorithms. Instead, these statuses are pre-configured in a comprehensive list or table that includes all possible component combinations. Initially, we assess whether each configuration meets the demand requirements. Among the feasible configurations, we then select the one that minimizes operational costs. This approach enables us to explore more efficient combinations of operational states (e.g., all MEs and DG1 are on, while the other DGs are off) for each algorithm.

A benchmark solution is used for the performance comparison, which is not optimal but meets the power demands, based on the experience and knowledge from previous projects and sailings. In this benchmark, the battery power is always set to 0, which means batteries are manually turned off when we do not use EMS. The results of all algorithms are compared to the benchmark and the difference percentages are calculated. The total power of all main engines is, theoretically, the sum of the demand for shaft power and losses.

Table 2: Benchmark outputs for three scenarios

Parameters	unit	Scenarios		
		1	2	3
Power output, port side main engine	kW	1823.227	3856.582	9100.000
Power output, starboard side main engine	kW	1823.227	3856.582	9100.000
Speed of the 1st diesel generator	rpm	2099.000	2099.000	2099.000
Speed of the 2nd diesel generator	Rpm	2099.000	0	0
Speed of the 3rd diesel generator	Rpm	2099.000	0	0
Speed of the 4th diesel generator	Rpm	0	0	0
Power output, 1st diesel generator	kW	550.768	1650	1677.627
Power output, 2nd diesel generator	kW	550.768	0	0
Power output, 3rd diesel generator	kW	550.768	0	0
Power output, 4th diesel generator	kW	0	0	0
Power output/input, 1st battery	kW	0	0	0
Power output/input, 2nd battery	kW	0	0	0

Due to the possibility of applying weight factors, tests are conducted not only with multiple scenarios but also with various combinations of weight factors. For the two-objective cases, the weight factor combinations range from 0.1 for fuel and 0.9 for LCC to 0.9 for fuel and 0.1 for LCC. A detailed example is provided for a weight factor combination of 0.5(50%) on fuel cost and 0.5(50%) on LCC, which is also defined as the OPEX mode. For the four-objective case, the weight factor combinations change in two patterns. In one pattern, fuel and LCC are paired and share the same values, while IR and noise are also paired and vary in the same manner. The other pattern involves a fixed weight factor set (0.1, 0.2, 0.3, and 0.4). One detailed example is given below for the balance mode (25% weight on each aspect).

It is noted that for the four-objective case, simulations were conducted using only the interior-point, active-set, and Nelder-Mead methods. The Lagrange method was not employed because it requires manual calculation of the derivatives of both the cost function and constraints. This process can be particularly challenging with nonlinear objective functions.

Table 3: Output of power sources using three algorithms in the OPEX weight-factor setting (50% on fuel, and 50% on LCC) of the two-objective case in scenario 1

Parameters	Unit	Lagrange	Interior point	Active set	Nelder Mead
Main Enginer power ps	kW	0.000	0.000	0.000	0.000
Main Enginer power stb	kw	3560.378	0.000	0.000	3288.803
Battery bank 1 power	kW	187.411	339.683	0.000	0.000
Battery bank 2 power	kW	187.411	339.683	0.000	0.000
Diesel generator 1 power	kW	1572.699	2317.982	1771.777	2176.790
Diesel generator 2 power	kW	0.000	2317.982	1771.777	0.000
Diesel generator 3 power	kW	0.000	0.000	1771.777	0.000
Diesel generator 4 power	kW	0.000	0.000	0.000	0.000
Diesel generator 1 speed	rpm	1724.230	2043.398	1894.506	1932.576
Diesel generator 2 speed	rpm	0.000	2043.398	1894.506	0.000
Diesel generator 3 speed	rpm	0.000	0.000	1894.506	0.000
Diesel generator 4 speed	rpm	0.000	0.000	0.000	0.000
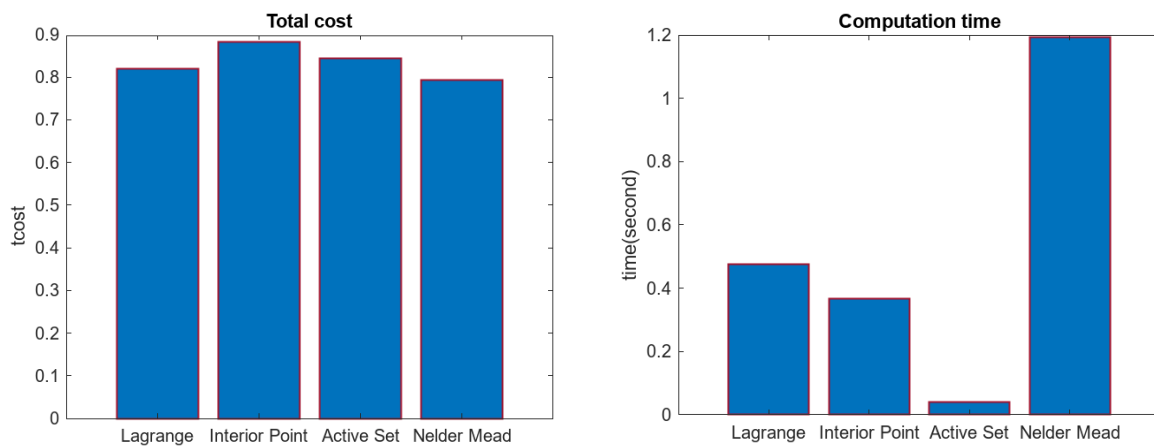
Scenario 1
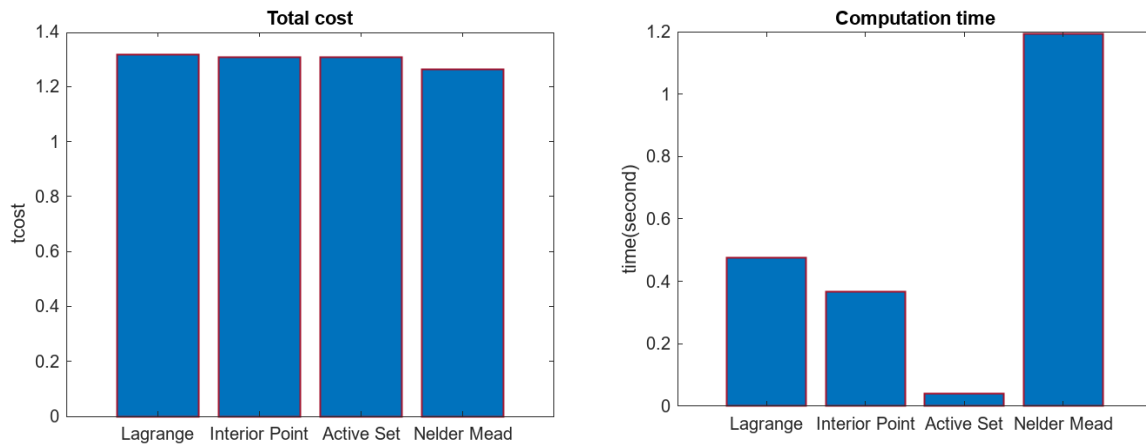
Scenario 2

Figure 8: One example of two-objective case - OPEX (weight factor 50% fuel 50% LCC)

Table 4: Output of power sources using three algorithms in the balance weight-factor setting (25% on fuel, 25% on LCC, 25% on IR, 25% on noise) of the four-objective case in scenario 1

| Parameters	Unit	Interior point	Active set	Nelder Mead
Main Enginer power ps	kW	0.000	0.000	0.000
Main Enginer power stb	Kw	0.000	0.000	0.000
Battery bank 1 power	kW	339.683	339.683	316.273
Battery bank 2 power	kW	339.683	339.683	316.273
Diesel generator 1 power	kW	2317.982	2317.982	2341.394
Diesel generator 2 power	kW	2317.982	2317.982	2341.390
Diesel generator 3 power	kW	0.000	0.000	0.000
Diesel generator 4 power	kW	0.000	0.000	0.000
Diesel generator 1 speed	rpm	2043.398	2043.398	2099.928
Diesel generator 2 speed	rpm	2043.398	2043.398	2099.928
Diesel generator 3 speed	rpm	0.000	0.000	0.000
Diesel generator 4 speed	rpm	0.000	0.000	0.000

Scenario 1

Scenario 2
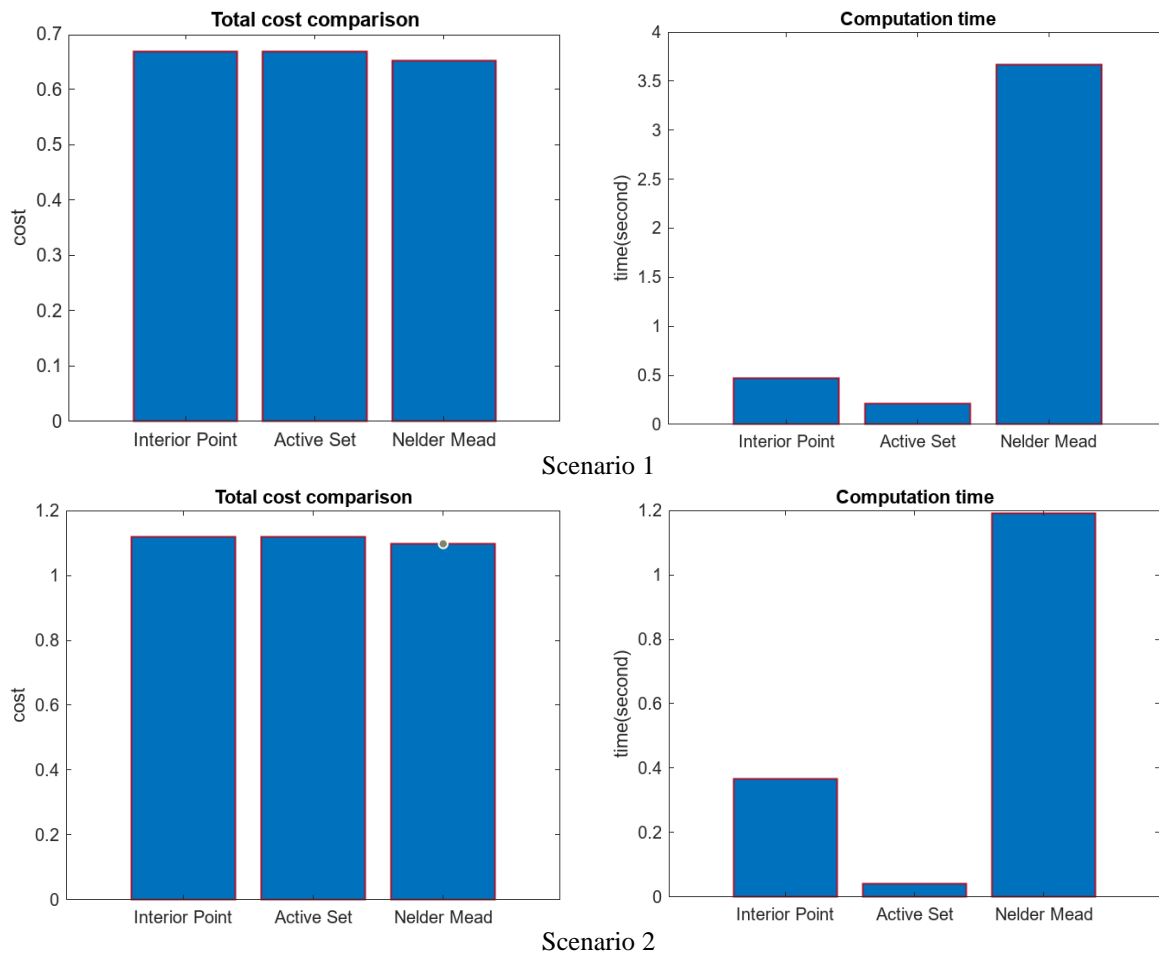
Figure 9: One example in four-objective – balance (weight factor 25% fuel 25% LCC 25% IR 25% noise)

5.2. Evaluation

The simulation results indicate that the Nelder-Mead method outperforms the Lagrange and two other methods in terms of cost in most cases. However, in certain scenarios, such as the two-objective case in scenario 1 with weight factors of 0.1 for fuel and 0.9 for LCC, the Nelder-Mead solution is not the most cost-effective (with interior-point and/or active-set methods performing better). Nevertheless, it seems that consistently performs better than the Lagrange method in all other cases. The improvement in cost efficiency between the Lagrange and Nelder-Mead methods ranges from approximately 1% to 8% across the tested cases.

The average computational time of the Nelder-Mead method is the longest in most cases. Occasionally, the interior-point method has the longest computational time (e.g., in scenario 5 with only the fuel objective), but this is not common. Although the Nelder-Mead method takes longer than the Lagrange method, the computation time remains within the acceptable limits for the EMS system's maximum desired calculation period of 60 seconds.

One limitation of the Lagrange method during this test is its case/model specificity. Particularly, when the cost function, equation, or constraints change, the derivatives must be updated accordingly. This becomes difficult with nonlinear models, as significant additional work is required due to its limitations in handling nonlinear cases. The fuel map used in this test comprises different regions, each with distinct coefficients or even different polynomials of varying orders. The Lagrange method cannot automatically switch among these regions, necessitating additional effort to specify the settings. In contrast, the Nelder-Mead method does not rely on derivatives, thereby reducing the need for additional work when introducing new cases, factors, or models. This makes it more adaptable for future changes.

Table 5: Total cost and computation time of the four algorithms with different weight factor combinations in two-objective optimization case of scenario 1

W_fuel	W_LCC	Reference cost	Lagrange		Interior point		Active set		Nelder Mead	
			Total cost	Comp. time	Total cost	Comp. time	Total cost	Comp. time	Total cost	Comp. time
0.1	0.9	1.1495	0.6689 (58.19%)	1.6742	**0.5790 (50.37%)**	0.4412	**0.5790 (50.37%)**	0.3847	0.5817 (50.61%)	4.4976
0.2	0.8	1.1682	0.7066 (60.48%)	1.7004	0.6451 (55.23%)	0.4108	0.6451 (55.23%)	0.3882	**0.6327 (54.16%)**	5.4334
0.3	0.7	1.1869	0.7443 (62.70%)	1.7053	0.7113 (59.93%)	0.4260	0.7113 (59.93%)	0.3743	**0.6836 (57.59%)**	3.9637
0.4	0.6	1.2057	0.7820 (64.86%)	1.7338	0.7774 (64.48%)	0.4863	0.7774 (64.48%)	0.3784	**0.7346 (60.93%)**	3.6676
0.5	0.5	1.2244	0.8197 (66.94%)	1.7153	0.8834 (72.15%)	0.6068	0.8436 (68.90%)	0.3802	**0.7940 (64.85%)**	4.7439
0.6	0.4	1.2431	0.8574 (68.97%)	1.7134	0.9263 (74.52%)	0.5075	0.9097 (73.18%)	0.3779	**0.8397 (67.55%)**	4.6157
0.7	0.3	1.2619	0.8951 (70.93%)	1.7068	0.9565 (75.80%)	0.5917	0.9565 (75.80%)	0.3848	**0.8918 (70.67%)**	4.0779
0.8	0.2	1.2806	0.9328 (72.84%)	1.7198	0.9358 (73.08%)	0.5969	0.9358 (73.08%)	0.3737	**0.9021 (70.44%)**	4.8002
0.9	0.1	1.2994	0.8333 (64.14%)	1.7208	0.9085 (69.92%)	0.8679	0.9085 (69.92%)	0.3273	**0.8240 (63.42%)**	6.6095

Table 6: Total cost and computation time of the four algorithms with different weight factor combinations in two-objective optimization case of scenario 2

W_fuel	W_LCC	Reference cost	Lagrange		Interior point		Active set		Nelder Mead	
			Total cost	Comp. time	Total cost	Comp. time	Total cost	Comp. time	Total cost	Comp. time
0.1	0.9	0.9258	0.9048 (97.73%)	0.3456	0.9090 (98.18%)	0.2671	0.9090 (98.18%)	0.1468	**0.8640 (93.33%)**	1.6474
0.2	0.8	1.0272	1.0076 (98.09%)	0.3492	1.0088 (98.21%)	0.2493	1.0088 (98.21%)	0.1404	**0.9881 (96.19%)**	1.4357
0.3	0.7	1.1286	1.1104 (98.39%)	0.3412	1.1086 (98.23%)	0.2969	1.1086 (98.23%)	0.1406	**1.0685 (94.67%)**	1.2300
0.4	0.6	1.2300	1.2132 (98.63%)	0.3443	1.2085 (98.25%)	0.2857	1.2085 (98.25%)	0.1434	**1.1606 (94.36%)**	1.2948
0.5	0.5	1.3314	1.3160 (98.84%)	0.3362	1.3083 (98.27%)	0.2633	1.3083 (98.27%)	0.1393	**1.2621 (94.80%)**	1.6161
0.6	0.4	1.4327	1.4188 (99.02%)	0.3530	1.4081 (98.28%)	0.2636	1.4081 (98.28%)	0.1437	**1.3507 (94.27%)**	1.2748
0.7	0.3	1.5341	1.5215 (99.18%)	0.3449	1.5080 (98.30%)	0.2726	1.5080 (98.30%)	0.1391	**1.4835 (96.70%)**	1.3350
0.8	0.2	1.6355	1.6243 (99.32%)	0.3464	1.6078 (98.31%)	0.2815	1.6078 (98.31%)	0.1400	**1.5439 (94.40%)**	1.1766
0.9	0.1	1.7369	1.7232 (99.21%)	0.3473	1.7076 (98.32%)	0.5049	1.7076 (98.32%)	0.1375	**1.6088 (92.63%)**	1.7600

Table 7: Total cost and computation time of the four algorithms with different weight factor combinations in two-objective optimization case of scenario 3

W_fuel	W_LCC	Reference cost	Lagrange		Interior point		Active set		Nelder Mead	
			Total cost	Comp. time	Total cost	Comp. time	Total cost	Comp. time	Total cost	Comp. time
0.1	0.9	1.1611	1.1532 (99.32%)	0.1509	1.1529 (99.29%)	0.3986	1.1552 (99.49%)	0.2217	**1.1489 (98.95%)**	1.2543
0.2	0.8	1.4341	1.4239 (99.29%)	0.1459	1.4226 (99.20%)	0.3728	1.4270 (99.50%)	0.2270	**1.4191 (98.95%)**	1.4445
0.3	0.7	1.7071	1.6946 (99.26%)	0.1654	1.6923 (99.13%)	0.4438	1.6986 (99.50%)	0.2144	**1.6920 (99.11%)**	1.1543
0.4	0.6	1.9802	1.9653 (99.25%)	0.1477	1.9620 (99.08%)	0.3877	1.9667 (99.32%)	0.2111	**1.9519 (98.57%)**	1.0586
0.5	0.5	2.2532	2.2359 (99.23%)	0.1522	2.2317 (99.05%)	0.3690	2.2354 (99.21%)	0.2198	**2.2266 (98.82%)**	1.3616
0.6	0.4	2.5262	2.5066 (99.22%)	0.1466	2.5015 (99.02%)	0.3580	2.5057 (99.19%)	0.2133	**2.4977 (98.87%)**	1.5435
0.7	0.3	2.7993	2.7773 (99.22%)	0.1507	2.7712 (99.00%)	0.3176	2.7748 (99.13%)	0.2211	**2.7700 (98.96%)**	1.3979
0.8	0.2	3.0723	3.0480 (99.21%)	0.1473	3.0409 (98.98%)	0.2859	3.0447 (99.10%)	0.2214	**3.0314 (98.67%)**	1.9626
0.9	0.1	3.3453	3.3186 (99.20%)	0.1459	3.3106 (98.96%)	0.3073	3.3145 (99.08%)	0.2216	**3.2139 (96.07%)**	2.2189

Table 8: Total cost and computation time of the four algorithms with different weight factor combinations in four-objective optimization case of scenario 1

Weight factor				Interior point		Active set		Nelder Mead	
W_fuel	W_LCC	W_noise	W_IR	Total cost	Time (s)	Total cost	Time (s)	Total cost	Time (s)
0.45	0.45	0.05	0.05	0.8402	0.5132	0.8093	0.2115	**0.7907**	3.3387
0.40	0.40	0.10	0.10	0.7969	2.3007	**0.7750**	0.4882	0.7865	3.7023
0.35	0.35	0.15	0.15	0.7537	0.4334	**0.7407**	0.1991	0.7510	4.0846
0.30	0.30	0.20	0.20	0.7015	0.4351	0.7064	0.1975	**0.6988**	3.2590
0.25	0.25	0.25	0.25	0.6673	0.5924	0.6673	0.1867	**0.6507**	3.4811
0.20	0.20	0.30	0.30	0.6240	0.4665	0.6240	0.1899	**0.6030**	3.3847
0.15	0.15	0.35	0.35	0.5808	0.4885	0.5808	0.1927	**0.5551**	2.6862
0.10	0.10	0.40	0.40	0.5376	0.4344	0.5376	0.1991	**0.5082**	3.6932
0.05	0.05	0.45	0.45	0.4944	0.9328	0.4944	0.2062	**0.4596**	2.7352
0.40	0.30	0.20	0.10	0.8203	0.4816	0.8203	0.2046	**0.8105**	3.9088
0.10	0.20	0.30	0.40	0.5142	0.3920	0.5142	0.1900	**0.4910**	2.8459

Table 9: Total cost and computation time of the four algorithms with different weight factor combinations in four-objective optimization case of scenario 2

Weight factor				Interior point		Active set		Nelder Mead	
W_fuel	W_LCC	W_noise	W_IR	Total cost	Time (s)	Total cost	Time (s)	Total cost	Time (s)
0.45	0.45	0.05	0.05	1.2703	0.2067	1.2703	0.0396	**1.2305**	1.2104
0.40	0.40	0.10	0.10	1.2324	0.2046	1.2324	0.0409	**1.2140**	1.1614
0.35	0.35	0.15	0.15	1.1944	0.2191	1.1944	0.0398	**1.1746**	1.1896
0.3	0.30	0.20	0.20	1.1565	0.2192	1.1565	0.0418	**1.1479**	1.1852
0.25	0.25	0.25	0.25	1.1185	0.2107	1.1185	0.0409	**1.0975**	0.9684
0.20	0.20	0.30	0.30	1.0806	0.2272	1.0806	0.0396	**1.0502**	1.3762
0.15	0.15	0.35	0.35	1.0426	0.2060	1.0426	0.0401	**1.0059**	1.4648
0.10	0.10	0.40	0.40	0.9563	0.3456	1.0047	0.0414	**0.9405**	0.9165
0.05	0.05	0.45	0.45	**0.8306**	1.4590	0.9581	0.0392	0.8410	1.2540

Table 10: Total cost and computation time of the four algorithms with different weight factor combinations in four-objective optimization case of scenario 3

Weight factor				Interior point		Active set		Nelder Mead	
W_fuel	W_LCC	W_noise	W_IR	Total cost	Time (s)	Total cost	Time (s)	Total cost	Time (s)
0.45	0.45	0.05	0.05	2.2149	0.3393	2.2185	0.1332	**2.2067**	1.1457
0.40	0.40	0.10	0.10	2.1981	0.3022	2.2015	0.0973	**2.1816**	1.0650
0.35	0.35	0.15	0.15	2.1813	0.3160	2.1845	0.0802	**2.1481**	1.1828
0.30	0.30	0.20	0.20	2.1320	0.9050	2.1674	0.0765	**2.1100**	1.0269
0.25	0.25	0.25	0.25	**1.9339**	1.6661	2.1502	0.0809	1.9897	1.4031
0.20	0.20	0.30	0.30	1.9247	0.8518	2.1330	0.0767	**1.8488**	1.4996
0.15	0.15	0.35	0.35	**1.6018**	1.6396	2.1156	0.0751	1.6499	1.5007
0.10	0.10	0.40	0.40	2.0973	0.2426	2.0983	0.0736	**1.4883**	1.2462
0.05	0.05	0.45	0.45	**1.2992**	1.5984	2.0810	0.0757	1.3108	1.3184

6.   Conclusions & Recommendations

Based on our findings, overall, Nelder Mead has the best performance in terms of the total cost optimization in the majority of cases, compared to the Lagrange multiplier and other two variants. Though in some cases, e.g. the two-objective case with weight factors of fuel and LCC as 0.1 and 0.9 combination, the solution of Nelder Mead is not the best cost wisely (interior-point and/or active-set is better), it is always better than the Lagrange. The improvement percentage between Lagrange and Nelder Mead is around 1-8% according to the cases tested.

The average computational time of Nelder Mead is longest in the most cases. Sometimes interior-point is the longest (only fuel objective, scenario 3) but this is not common. Though the time is longer than the Lagrange, this duration still remains within the acceptable bounds for the EMS system's maximum desired calculation period (60 seconds).

One limitation of the Lagrange that became apparent during this test is that it is case/model specific. Especially, when the cost function or the constraints change, the derivatives need to be re-formulated. And when there are nonlinear models, more work needs to be performed additionally, such as linearization of non-linear models since Lagrange is limited in non-linear cases. The fuel map used in this test has different regions. In each region, different coefficients or even different polynomials with different orders are used. The Lagrange multiplier method cannot switch automatically among these regions and additional work needs to be done to specify the settings. On the

contrary, Nelder Mead does not use derivatives and thus does not require for much additional work when new cases or models need to be used, which makes it more general for future changes.

Considering the current results, our conclusion is adopting a hybrid approach: executing multiple algorithms simultaneously, either across separate cores in a centralized system or on distinct computers in a distributed setup, would be optimal. This would utilize the strengths of each method, aiming for the best outcome. Given the computational power we would have, this strategy is feasible.

As an alternative methodology, when one algorithm is used, in order to minimize the risk, one could consider enhancing the Lagrange or the other two methods with a high-level pre-configuration layer. This layer would determine specific operational regions and the on/off status of the MEs and DGs. Such an approach could align closely with the expectations of on board crew who have predefined requirements. This would allow to perform optimizations within these set parameters, potentially fulfilling stakeholder's needs more effectively.

Acknowledgements

References

Mitropoulou, D., Kalikatzarakis, M., Van Der Klauw, T., Blockland, A. Geertsma, R., Bucurenciu, A., Dembinskas, D. 2020. Multi-objective optimization and Energy Management: adapt your ship to every mission, in: Proceedings of the 16th international naval engineering conference, pp. 1–12.

Barton, R.R., Ivey Jr, J.S., 1996. Nelder-mead simplex modifications for simulation optimization. Management Science 42, 954–973.

Breijs, A., Amam, E., 2016. Energy management–adapt your engine to every mission, in: Proceedings of the 13th international naval engineering conference, pp. 1–8.

Geertsma, R., Negenborn, R., Visser, K., Hopman, J., 2017. Design and control of hybrid power and propulsion systems for smart ships: A review of developments. Applied Energy 194, 30–54.

Kalikatzarakis, M., Geertsma, R., Boonen, E., Visser, K., Negenborn, R., 2018. Ship energy management for hybrid propulsion and power supply with shore charging. Control Engineering Practice 76, 133–154.

Li, J., Xiong, R., Yang, Q., Liang, F., Zhang, M., Yuan, W., 2017. Design/test of a hybrid energy storage system for primary frequency control using a dynamic droop method in an isolated microgrid power system. Applied Energy 201, 257–269.

Mitropoulou, D., Elling, L., 2018. New developments in energy management-battery lifetime incorporation and power consumption forecasting, in: Proceedings of the 14th international naval engineering conference, pp. 1–12.

Sciarretta, A., Serrao, L., Dewangan, P., Tona, P., Bergshoeff, E., Bordons, C., Charmpa, L., Elbert, P., Eriksson, L., Hofman, T., et al., 2014. A control benchmark on the energy management of a plug-in hybrid electric vehicle. Control engineering practice 29, 287–298.

Sundstrom, O., Guzzella, L., 2009. A generic dynamic programming matlab function, in: 2009 IEEE control applications,(CCA) & intelligent control,(ISIC), IEEE. pp. 1625–1630.

van Vugt, H., Sciberras, E., de Vries, L., Heslop, J., Roskilly, A.P., 2016. Ship power system modelling for the control and optimisation of multiple alternative energy sources on-board a ship, in: Proc. 15th Int. Conf. Comput. IT Appl. Martime Ind. (COMPIT), pp. 240–254.